Open access • Journal Article • DOI:10.1029/JA077I001P00076

High-frequency electromagnetic response of the Moon — Source link

Gerald Schubert, K. Schwartz

Institutions: University of California, Los Angeles

Published on: 01 Jan 1972 - Journal of Geophysical Research (John Wiley & Sons, Ltd)

Topics: Harmonics and Magnetic field

HIGH FREQUENCY ELECTROMAGNETIC RESPONSE OF THE MOON

G. Schubert

Department of Planetary and Space Science
University of California
Los Angeles, California
90024

K. Schwartz

American Nucleonics Corporation
Woodland Hills, California
91364

ABSTRACT

It is shown that the contribution of higher harmonics to the lunar transfer functions for the tangential components of the surface magnetic field is significant at frequencies greater than 0.01 Hz (Apollo 12-Explorer 35 magnetometer data extend to frequencies as high as 0.04 Hz). The inclusion of the higher harmonics shows that there are two distinct transfer functions corresponding to the components of the tangential surface magnetic field perpendicular and parallel to the direction of the wave vector of the external disturbance forcing the lunar induction. The dependences of these transfer functions on frequency and location are determined. The effects of the higher harmonics can 1) account for a hitherto unexplained feature in the Apollo 12-Explorer 35 transfer functions, namely the rolloff at high frequencies and 2) offer a possible explanation for the frequency dependence of the difference between the transfer functions for the two orthogonal components of the surface magnetic field. The harmonic response of a simple current layer model of the Moon is derived and shown to provide a reasonable fit to the experimental data.

INTRODUCTION

The Apollo 12 Lunar Surface Magnetometer (LSM) experiment has stimulated considerable theoretical investigation into the interaction between the Moon and magnetic field fluctuations in the solar wind. The Moon-solar wind magnetic field interaction can be characterized by transfer functions for the components of magnetic field tangent to the lunar surface, i.e. the ratios of the tangential magnetic field components at the lunar surface to the tangential components of the solar wind magnetic forcing field. Previous approximations to these transfer functions [Blank and Sill, 1969] are valid only at low frequencies and thus have been unable to account for the high frequency rolloff of the experimental lunar transfer functions (see Figure 1, in particular the frequency range 0.01 - 0.04 Hz). It will be shown that at high frequencies the transfer functions for the two orthogonal tangential magnetic field components are in fact different, dependent on position on the surface of the Moon, and can exhibit rolloff at high frequency. The behavior, with frequency, of the difference between the transfer functions for the two orthogonal components of the tangential magnetic field can be understood by the high frequency effects to be discussed in this paper.

In the following section we outline the theory leading to the definitions of the tangential magnetic field transfer functions

and discuss their relationship to the low frequency approximations. Transfer functions are then presented for several lunar electrical conductivity models and are qualitatively compared to the experimental data.

LUNAR RESPONSE TO INDUCTION BY THE SOLAR WIND

A complete solution of the electromagnetic interaction between the solar wind and the Moon requires that one solve a complex magnetohydrodynamic flow problem external to the Moon coupled with the matching at the lunar surface of the electromagnetic fields in the Moon's interior. An approximate solution for the sunlit side of the Moon can be obtained because of the experimental observation that the solar wind flow shows no marked perturbations except for the diamagnetic cavity and the apparently minor after body shocks at the cavity-solar wind boundary [Colburn et al., 1971]. To a first approximation, the effects of the cavity are negligible on the sunlit lunar hemisphere where, in addition, the dynamic pressure of the solar wind is effective in confining induced magnetic fields to the interior of the Moon [Sonett et al., 1971a,b]. Thus as in previous analyses [Blank and Sill, 1969; Schubert and Schwartz, 1969], the electromagnetic Moon-solar wind interaction problem for the sunlit hemisphere will be solved by assuming that the Moon is immersed within a perfectly conducting space. Physically,

the induced dayside field will be confined by an external current layer above the lunar surface. By placing the perfectly conducting space at the lunar surface, it is assumed that the thickness of the confining current layer is small compared to the depth at which lunar induction currents flow. The adequacy of this approximation can be assessed by noting how closely the transfer function for the component of magnetic field normal to the lunar surface approaches unity. [Sonett et al., 1971a]. The Apollo 15 subsatellite magnetometer, which will sample the magnetic field at altitudes of less than 100 km above the lunar surface, may be expected to clarify the nature of the confining current layer.

Following the development in Sonett et al. [1971a], the solar wind forcing magnetic field oscillation is written in the form

$$\underline{H} = \hat{\underline{\eta}} H_0 \exp 2\pi i(\zeta/\lambda - ft) \quad , \qquad (1)$$

where the Cartesian coordinate system (ξ,η,ζ) with unit vectors $(\hat{\underline{\xi}},\hat{\underline{\eta}},\hat{\underline{\zeta}})$ is fixed in the Moon with its origin at the Moon's center (Figure 2). The quantities H_0 , λ and f are the amplitude, wavelength and frequency, respectively, of the magnetic field oscillation propagating in the positive ζ-direction.

Sonett et al. [1971a] have shown that the lunar magnetic response is primarily a transverse electric one with magnetic field components (for the total magnetic field) which can be written in the form (aside from the factor $e^{-2\pi i f t}$)

$$H_r = H_0 \sin\varphi \sum_{\ell=1}^{\infty} \beta_\ell \frac{\lambda a}{2\pi i r} j_\ell \left(\frac{2\pi a}{\lambda}\right) \ell(\ell+1) \left(\frac{G_\ell}{r}\right) P_\ell^1 (\cos\theta), \qquad (2)$$

$$\begin{Bmatrix} H_\theta \\ H_\varphi \end{Bmatrix} = H_0 \begin{Bmatrix} \sin\varphi \\ \cos\varphi \end{Bmatrix} \sum_{\ell=1}^{\infty} \beta_\ell \frac{\lambda a}{2\pi i r} j_\ell \left(\frac{2\pi a}{\lambda}\right) \frac{dG_\ell}{dr} \begin{Bmatrix} \dfrac{dP_\ell^1 (\cos\theta)}{d\theta} \\ P_\ell^1(\cos\theta)/\sin\theta \end{Bmatrix}, \qquad (3)$$

where (r,θ,φ) are spherical coordinates with the polar axis along ζ and $r=a$ is the lunar surface (see Figure 2), j_ℓ are the spherical Bessel functions,

$$\beta_\ell = \frac{i^\ell (2\ell+1)}{\ell(\ell+1)} \quad , \qquad (4)$$

$P_\ell^1 (\cos\theta)$ are the Legendre functions and $G_\ell (r)$ are determined from the radial differential equations

$$\frac{d^2 G_\ell}{dr^2} + \left\{k^2 - \frac{\ell(\ell+1)}{r^2}\right\} G_\ell (r) = 0 \quad , \qquad (5)$$

with

$$k^2 = \omega^2 \mu\varepsilon + i\omega\mu\sigma \quad , \qquad \omega = 2\pi f \quad , \qquad (6)$$

and

$$G_\ell(r=0) \text{ finite}, \quad G_\ell(r=a) = 1$$

The parameters μ and ϵ are the magnetic permeability and electric permittivity, respectively, and σ is the electrical conductivity which is assumed to be an arbitrary function of radius. For the present work, free space values for μ and ϵ have been assumed and MKS units are used throughout.

For completeness we also present the spherical harmonic expansion for the TE portion of the incident magnetic field (aside from the factor $e^{-i\omega t}$)

$$H_r = H_0 \sin\varphi \sum_{\ell=1}^{\infty}{}' \beta_\ell \frac{\lambda}{2\pi i r} \ell(\ell+1)\, j_\ell\left(\frac{2\pi r}{\lambda}\right) P_\ell^1(\cos\theta)$$

$$\begin{Bmatrix} H_\theta \\ H_\varphi \end{Bmatrix} = H_0 \begin{Bmatrix} \sin\varphi \\ \cos\varphi \end{Bmatrix} \sum_{\ell=1}^{\infty}{}' \beta_\ell \frac{\lambda}{2\pi i r} \frac{d}{dr}\left(r j_\ell\left(\frac{2\pi r}{\lambda}\right)\right) \begin{Bmatrix} \dfrac{dP_\ell^1(\cos\theta)}{d\theta} \\ \dfrac{P_\ell^1(\cos\theta)}{\sin\theta} \end{Bmatrix}. \qquad (7)$$

The transfer functions for the tangential magnetic field components can now be defined by decomposing the forcing field (1) into its components in the spherical polar coordinate system and forming the ratio, component by component, of the total tangential field components (3) to those of the forcing field.

The magnitude of the transfer functions for the θ and φ components at the lunar surface (r=a) are

$$\begin{Bmatrix} T_\theta \\ T_\varphi \end{Bmatrix} = \left| \sum_{\ell=1}^{\infty} \beta_\ell \frac{\lambda}{2\pi i} j_\ell \left(\frac{2\pi a}{\lambda}\right)\left(\frac{dG_\ell}{dr}\right)_{r=a} \begin{Bmatrix} \frac{dP_\ell^1(\cos\theta)}{\cos\theta \, d\theta} \\ \frac{P_\ell^1(\cos\theta)}{\sin\theta} \end{Bmatrix} \right| . \qquad (8)$$

The transfer functions depend on the colatitude angle θ but are independent of azimuth φ. We now define the point where $\theta = \pi$ as the sub-k point, i.e., the point at which the wave vector is normal to and into the lunar surface. At the sub-k point

$$\frac{1}{\cos\theta} \frac{dP_\ell^1(\cos\theta)}{d\theta} = \frac{P_\ell^1(\cos\theta)}{\sin\theta} ,$$

and therefore

$$T_\theta \ (\theta=\pi) = T_\varphi(\theta=\pi) .$$

Sonett et al. [1971a] have defined a transfer function as the ratio, term by term, of the tangential magnetic field given by (3) to the driving field given by (7). This definition provides a transfer function for each harmonic which is independent of θ and φ and which is the same for both tangential components

$$T^{\ell} = \left\{ \frac{r\left(\frac{dG_{\ell}}{dr}\right) j_{\ell}\left(\frac{2\pi r}{\lambda}\right)}{\frac{d}{dr}\left(r j_{\ell}\left(2\pi r/\lambda\right)\right)} \right\}_{r=a} \quad . \tag{9}$$

It is difficult to interpret the experimental data in terms of the transfer functions T^{ℓ} because of the present inability to separate the data into individual harmonic contributions. We will see that for $f \lesssim 0.01$ Hz, $T^1 \approx T_\theta \approx T_\varphi$.

Approximations to the transfer functions T_θ and T_φ have appeared in the literature. Blank and Sill [1969] assumed a spatially uniform forcing magnetic field of the form $\underline{H} = \hat{\underline{n}} H_0 e^{-i\omega t}$ (in our notation) and thus considered a transfer function, which we refer to as T_0 , that can be obtained from (8) by taking the limit $2\pi a/\lambda \to 0$. The approximate transfer function T_0 is related to T^1 by

$$T_0 = \frac{1}{2} T^1 \left\{ \frac{\frac{2\pi a}{\lambda} j_0\left(\frac{2\pi a}{\lambda}\right)}{j_1\left(\frac{2\pi a}{\lambda}\right)} - 1 \right\} \quad . \tag{10}$$

The approximation T_0 is valid at low frequencies, but at frequencies greater than 0.01 Hz we will show that it departs significantly from (8). Since the experimental Apollo 12 LSM-Explorer 35 transfer functions are known at frequencies as high as 0.04 Hz, (8) is presently being used in the inversion of that data.

Three simple lunar electrical conductivity models will be used to illustrate the angular dependence of the tangential magnetic field transfer functions and to reveal the inadequacies of the approximation T_0 at frequencies greater than 0.01 Hz. The first is a two layer model with a perfectly conducting core of radius b surrounded by an insulating shell. The second model is also a two layer moon but with a finitely conducting core. The third is a moon of zero conductivity except for a thin conducting shell of conductivity σ and thickness δ centered at r=b. This model is suggested by the results of Sonett et al. [1971a,b], who inferred a near surface "spike" in electrical conductivity by inverting the combined Apollo 12 LSM and Explorer 35 harmonic data. To further simplify this model we assume that $\delta \to 0$ while $\sigma\delta$ remains constant; the thin conducting shell is thus represented by surface currents at r=b.

TWO LAYER MOON WITH A PERFECTLY CONDUCTING CORE AND INSULATING SHELL

For this model, the contribution to the transfer function (8) of the radially dependent term is

$$\left(\frac{dG_\ell}{dr}\right)_{r=a} = \frac{1}{a}\left\{\frac{\ell+1 + \ell(b/a)^{2\ell+1}}{1 - (b/a)^{2\ell+1}}\right\} \quad . \qquad (11)$$

If the conducting core is large, i.e. $1-b/a \ll 1$, the right hand side of (11) reduces to $(a-b)^{-1}$, a result which is independent of ℓ and thus allows the following numerical example to be scaled to other values of b.

The transfer functions T_θ and T_φ have been calculated for b = 1505 km over the frequency range $0 \leq f \leq 0.04$ Hz. The upper frequency corresponds to the highest frequency for which transfer functions are obtainable in the Apollo 12 LSM-Explorer 35 magnetometer experiment and the choice of b was motivated by the radial location of the near surface conductivity "spike" reported in Sonett et al. [1971a,b]. The computations assumed a wave propagation velocity of 400 km/sec and were carried out for a range of angles from $\theta = \pi$, the sub-k point, to $\theta = 2\pi/3$. Calculations were not carried out for $\theta < 2\pi/3$ since the assumption of induced field line confinement is expected to be best realized near the sub-solar point which we assume to be

near the sub-k point. Results for T_θ are shown in Figure 3. For the values of θ investigated here, T_φ is rather insensitive to changes in θ, i.e. $T_\varphi \approx T_\varphi\ (\theta=\pi) = T_\theta(\theta=\pi)$. The transfer functions T_θ show a rolloff with increasing frequency for $\theta \geq 130°$, the rolloff being greatest at the sub-k point. The transfer functions do not approach unity as $f \to 0$ because of the assumption of infinite core conductivity. For any finite value of electrical conductivity the transfer functions indeed approach unity as $f \to 0$. Since T_θ is relatively sensitive to θ, while T_φ is not, one should expect a difference between the values of the two experimental transfer functions for LSM locations not coincident with the sub-k point. The transfer function T^1 (also shown in Figure 3) is a monotonically increasing function. The approximate transfer function T_0 is independent of both angle and frequency and is given by

$$T_0 = \frac{1 + \frac{1}{2}(b/a)^3}{1 - (b/a)^3} \qquad (12)$$

This is the low frequency limit of T^1. For the case illustrated in Figure 3, (12) would give a straight line at 3.75.

TWO LAYER MOON WITH CORE OF FINITE CONDUCTIVITY σ_c AND AN INSULATING SHELL

The radially dependent term for this model is

$$\left(\frac{dG_\ell}{dr}\right)_{r=a} = \frac{1}{a} \cdot \frac{\ell+1 + \ell(b/a)^{2\ell+1} B_\ell(k_c b)}{1 - (b/a)^{2\ell+1} B_\ell(k_c b)} , \qquad (13)$$

where $k_c^2 = k^2(\sigma=\sigma_c)$, $r = b$ is the core radius, and

$$B_\ell(k_c b) = 1 - \frac{(2\ell+1)\, j_\ell\,(k_c b)}{k_c b\, j_{\ell-1}\,(k_c b)} . \qquad (14)$$

Both T_θ and T_φ were calculated as functions of f and θ for the case b = 1566 km and $\sigma_c = 10^{-3}$ mhos/m, the best 2-layer fit to the experimental transfer functions reported by Sonett et al. [1971a]. The results for T_θ are shown in Figure 4. As in the previous case T_φ showed only minor variation with θ for $\pi \leq \theta \leq 2\pi/3$. The function T_θ increases from unity at f = 0 and rolls off above 0.03 Hz for $\theta > 140°$. For $120° < \theta < 140°$, T_θ is monotonically increasing. As in the previous case we expect a difference between the two experimental transfer functions when LSM is not at the sub-k point. The function T^1 (the broad dashed line in Figure 4) is again monotonically increasing. The approximation T_0, also shown in Figure 4, tends to lie in the region of the figure which corresponds to T_θ for $\theta = 130°$ and is inaccurate at $f \geq 0.01$ Hz.

NONCONDUCTING MOON WITH THIN CURRENT LAYER

Sonett et al. [1971a,b] have reported a near surface shell of high electrical conductivity imbedded within a relatively insulating Moon except perhaps for a small conducting core. Thus, transient eddy currents in the Moon are concentrated mainly in this highly conducting thin shell. A mathematical idealization of these findings is a nonconducting Moon containing a current layer of negligible thickness situated at $r = b$ and characterized by a nonzero value of the product $\sigma\delta$.

Solutions of (5) with $k^2 \approx 0$ are proportional to $r^{-\ell}$, $r^{\ell+1}$. In the region $0 \leq r < b$ the solution proportional to $r^{-\ell}$ must be discarded and we find

$$G_\ell = A_\ell\, r^{\ell+1} \qquad 0 \leq r < b$$

$$= C_\ell\, r^{-\ell} + D_\ell\, r^{\ell+1}, \; b < r \leq a \qquad (15)$$

From boundary condition (6) and the continuity of the radial component of the magnetic field at $r = b$ we obtain

$$C_\ell\, a^{-\ell} + D_\ell\, a^{\ell+1} = 1 \qquad (16)$$

$$A_\ell = C_\ell\, b^{-2\ell-1} + D_\ell \qquad (17)$$

The additional boundary condition required to determine the solution follows from the fact that the jump in the tangential magnetic field is equal to the surface current density at r = b

$$\lim_{\delta \to 0} \quad H_\theta(r=b+\tfrac{\delta}{2}) - H_\theta(r=b-\tfrac{\delta}{2}) = \sigma\delta E_\varphi(r=b) \quad . \tag{18}$$

For the TE mode, the electric field component E_φ may be found by integrating the θ-component of the Maxwell equation $\nabla \times \underline{E} = -\partial \underline{B}/\partial t$ and noting that $E_r = 0$ and H_θ is given by (3). The result is

$$E_\varphi = -\mu\lambda f H_0 \sin\varphi \sum_{\ell=1}^{\infty} \beta_\ell \frac{a}{r} j_\ell \left(\frac{2\pi a}{\lambda}\right) G_\ell \frac{dP_\ell^1(\cos\theta)}{d\theta} \quad , \tag{19}$$

and from (3), (15), (18) and (19) we obtain

$$(\ell+1)D_\ell - \ell C_\ell b^{-2\ell-1} = A_\ell\{\ell+1 - 3i\omega\tau\} \quad , \tag{20}$$

where $\tau = \sigma\mu\delta b/3$, (21)

has been shown to be the appropriate time constant (Cowling decay time) of the current layer model for response in vacuum to an abrupt change in a spatially uniform magnetic field [Schubert and Colburn, 1971]. Combining (16), (17), and (20) we find that the radially dependent term, evaluated at r=a, is

$$\left(\frac{dG_\ell}{dr}\right)_{r=a} = \frac{1}{a} \frac{\ell+1 + \ell\left(\frac{b}{a}\right)^{2\ell+1} B_\ell(3i\omega\tau)}{1 - \left(\frac{b}{a}\right)^{2\ell+1} B_\ell(3i\omega\tau)} \quad , \tag{22}$$

$$\text{where} \quad B_\ell(3i\omega\tau) = \left(1 - \frac{2\ell+1}{3i\omega\tau}\right)^{-1} \quad . \tag{23}$$

The radially dependent term defined by (22) is formally identical to the one for the two layer Moon with a conducting core and an insulating shell, (13). The difference between the two lies in the definitions of $B_\ell(3i\omega\tau)$ and $B_\ell(k_c b)$. If $\omega\tau$ and $k_c b$ become infinite, both (13) and (22) reduce to (11), the radially dependent term for the two layer Moon with a perfectly conducting core and an insulating shell.

The illustrative model has the conducting layer at b = 1505 km and the product $\sigma\delta$ = 150 mhos. This latter quantity corresponds, for example, to a 50 km wide layer with a conductivity of 3×10^{-3} mhos/m. The approximation T_0 and the transfer functions T_θ and T^1 for this case are shown in Figure 5. As in the previous two cases, T_φ is relatively insensitive to variations in θ and is not shown in the Figure. The transfer function T_θ is sensitive to θ variations and also exhibits two characteristics which are significantly different from those of the two layer model with a finitely conducting core (Figure 4). First, consider the low frequency ($f \leq 0.0075$ Hz) region of the first curves. Both transfer functions (Figures 4 and 5) reach a magnitude of 3 at f = 0.00625 Hz. The current layer

response is almost linear between f = 0 and f = 0.00625 Hz whereas the two layer model shows a much more rapid rise which is turning over when $T_\theta = 3$. This difference was pointed out by Sonett et al. [1971a] in their discussion of the inadequacies of models other than their proposed conductivity profile. The second characteristic of the current layer model is the flattening of its response at a much lower frequency, $f \sim 0.015$ Hz, as compared to the two layer model which just barely flattens at f = 0.03 Hz. In Figure 5,

$$\overline{T} = \left\{\frac{1}{2}\left(T_z^2 + T_y^2\right)\right\}^{\frac{1}{2}}$$

from Sonett et al. [1971a,b], is shown with its error bars. The simple current layer model provides an excellent fit to the data at the lowest frequencies and is well within the error bars over most of the range $0.001 \leq f \leq 0.04$ Hz. It should be noted that the data points represent averages of observations at presently unknown values of θ, since identification of θ would require empirical knowledge of the distribution of the wave propagation vectors of the disturbances forcing the lunar induction.

CONCLUSIONS

It has been shown that there are two distinct transfer functions corresponding to the two orthogonal magnetic field components tangent to the Moon's surface; they are identical at the sub-k point but exhibit different functional behavior on the colatitude angle θ. One transfer function, T_φ, is relatively insensitive to θ while the other, T_θ, shows marked change as the colatitude angle decreases. Both functions show a significant high frequency rolloff for $\theta > \frac{5}{6}\pi$ but T_θ changes to a monotonically increasing function between $\theta = \frac{5}{6}\pi$ and $\theta = \frac{2}{3}\pi$. The limitations of the low frequency approximation T_0 have been made quantitative by the exact theory of this paper.

The present calculations provide an explanation for one of the unexpected features of the experimental transfer functions, namely a rolloff at the high frequency ($f > .025$ Hz) end of the spectrum (see Figure 1). This rolloff could not be understood on the basis of the approximation T_0 to the theoretical transfer functions. Neither does the transfer function T^1 exhibit a high frequency rolloff. The analysis of this paper shows that T_θ and T_φ do roll off at high frequencies if the observer is near the sub-k point. This phenomenon can be understood as follows. The relatively large magnitudes of the lunar transfer

functions result from the compression of induced magnetic fields into a shell between the confining solar wind and an inner "core" which excludes field lines at sufficiently high frequency. All the harmonics in (8) are thus amplified, however, the effect is of decreasing importance as one proceeds to higher harmonics, i.e. T^{ℓ} decreases with increasing ℓ at fixed f. Since the higher harmonics contribute proportionately more to the field at higher frequencies, i.e. since the power in the field is redistributed so that at higher frequencies relatively more power resides in the higher harmonics, the net effect is a rolloff in the amplification or transfer function.

That the rolloff is a function of proximity to the sub-k point is also clear from (8) if one notes that the contribution of each harmonic is proportional to either $\frac{1}{\cos\theta}\frac{dP_{\ell}^{1}}{d\theta}$ or $\frac{1}{\sin\theta}P_{\ell}^{1}$. For $\ell = 1$ these factors are both unity whereas for $\ell = 3$ (the harmonics $\ell = 1$ and $\ell = 3$ are approximately in phase) they are $\frac{3}{2}(4 - 15\sin^2\theta)$ and $\frac{3}{2}(4 - 5\sin^2\theta)$, respectively. As θ decreases from the value π, both these factors decrease, the first more rapidly, which accounts for the sensitivity of T_{θ} on θ and the relative insensitivity of T_{φ} on θ.

One final point concerns the observed asymmetry in the experimental data. Sonett et al. [1971a] showed data in which the Z-transfer function, corresponding to local north or

approximately perpendicular to the ecliptic, was in general, greater than the Y-transfer function, local east (Figure 1). The Z-transfer function corresponds to T_φ in this paper and the Y-transfer function corresponds to T_θ (assuming the wave vector lies in the equatorial plane). From the theoretical analysis, based only on a TE mode interaction, $T_\theta \geq T_\varphi$ and at frequencies below 0.01 Hz, $T_\theta \approx T_\varphi$ for all values of θ. The asymmetry in the data is nevertheless present even at the lowest frequencies, which indicates that the asymmetry must be attributed to some other cause, for example the presence of a TM mode or an asymmetry in the lunar conductivity distribution. Because of the way in which T_θ depends on f and θ we expect the basic asymmetry to decrease with frequency, a result confirmed by the data (Figure 1).

Acknowledgments. This report is based on NASA CR prepared for Ames Research Center under NASA Contract NAS2-5876.

REFERENCES

Blank, J.L. and W.R. Sill, Response of the Moon to the time-varying interplanetary magnetic field, J. Geophys. Res., 74, 736-743, 1969.

Colburn D.S., J.D. Mihalov and C.P. Sonett, Magnetic observations of the lunar cavity, J. Geophys. Res., 76, 2940-2957, 1971.

Schubert, G. and K. Schwartz, A theory for the interpretation of lunar surface magnetometer data, The Moon, 1, 106-117, 1969.

Schubert, G. and D.S. Colburn, Thin highly conducting layer in the Moon: Consistent interpretation of day and night-side electromagnetic responses, submitted to J. Geophys. Res., 1971.

Sonett, C.P., G. Schubert, B.F. Smith, K. Schwartz and D.S. Colburn, Lunar electrical conductivity from Apollo 12 magnetometer measurements: compositional and thermal inferences, Proc. Apollo 12 Lunar Science Conf., Geochim. Cosmochim. Acta. Suppl., in press, 1971a.

Sonett, C.P., D.S. Colburn, P. Dyal, C.W. Parkin, B.F. Smith, G. Schubert and K. Schwartz, Lunar Electrical conductivity profile, Nature, 230, 359-362, 1971b.

FIGURE CAPTIONS

Figure 1. Magnitude of the Apollo 12-Explorer 35 tangential transfer functions vs. frequency (from Sonett et al., 1971a). The Y component is east and the Z component north at the Apollo 12 site. Note the rolloff at the high frequencies and the differences in the transfer functions for the two tangential components.

Figure 2. The geometry of the lunar induction problem. The wave propagation direction of the external disturbance forcing the lunar response is in the ζ-direction. The angle θ is the colatitude of LSM with respect to the direction of the wave vector.

Figure 3. The transfer function T_θ and the approximation T^1 vs. frequency for a model Moon with an insulating shell and a core of infinite conductivity with radius 1505 km.

Figure 4. The transfer functions T_θ and T^1 and the approximation T_0 vs. frequency for a model Moon with an insulating shell and a core of radius 1566 km and uniform conductivity 10^{-3} mhos/m. Note the rolloff in T_θ at high frequency for $\theta > 140°$. The approximation T_0 is inaccurate at $f \geq 0.01$ Hz.

Figure 5. Theoretical transfer functions for a model Moon which is insulating except for a current layer at 1505 km with $\sigma\delta$ = 150 mhos. The data shown (points with associated standard deviations) are values of

$$\bar{T} = \left\{\frac{1}{2}\left(T_Z^2 + T_Y^2\right)\right\}^{\frac{1}{2}}$$

from Sonett et al. [1971a,b]. The current layer model provides an excellent fit to the data at the lowest frequencies and a reasonable fit at the high frequencies considering that the data represent averages of observations at unknown values of θ .

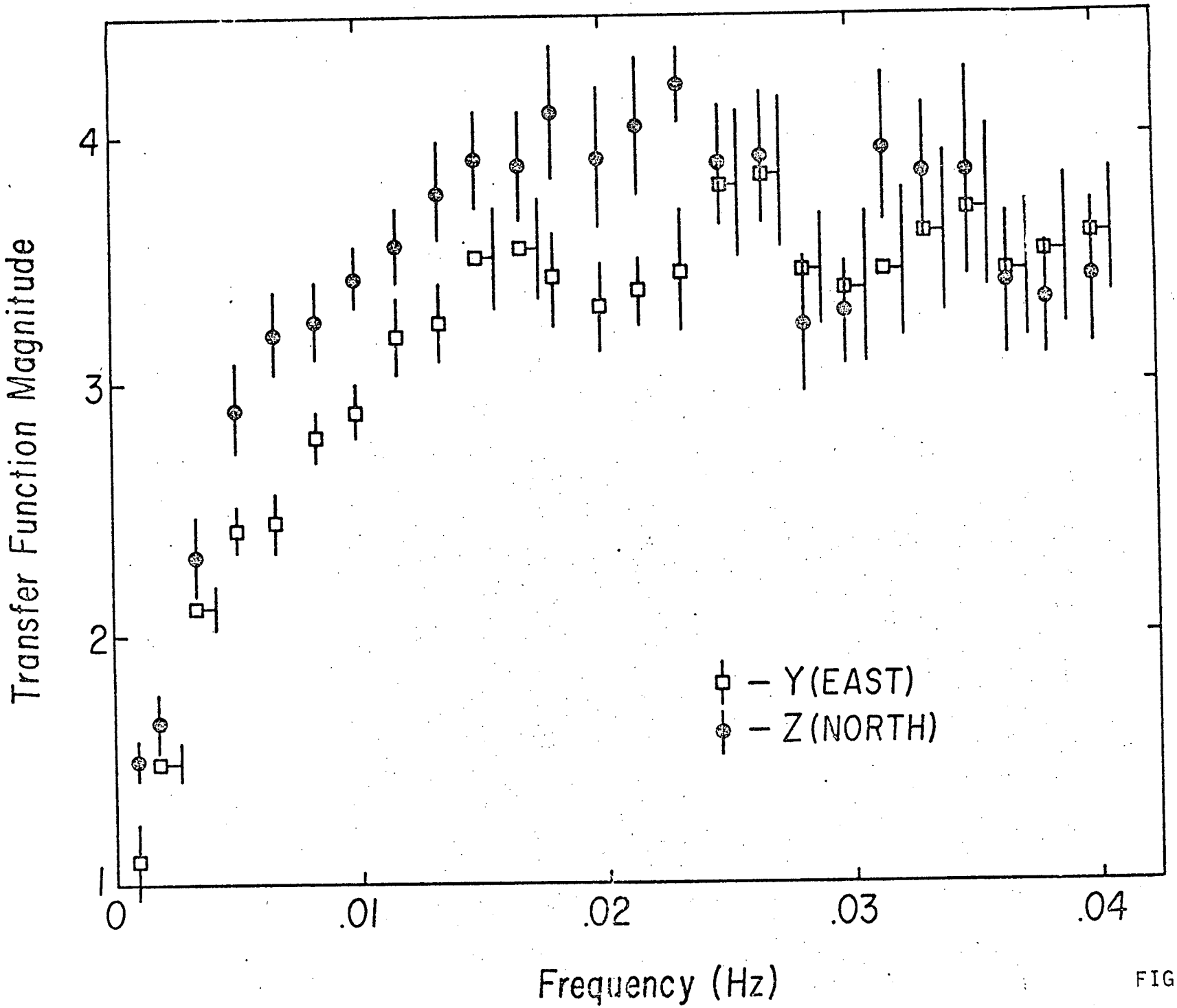
Transfer Function Magnitude
4
3
2
1
0
.01
.02
.03
.04
Frequency (Hz)
– Y(EAST)
– Z(NORTH)

FIG. 1

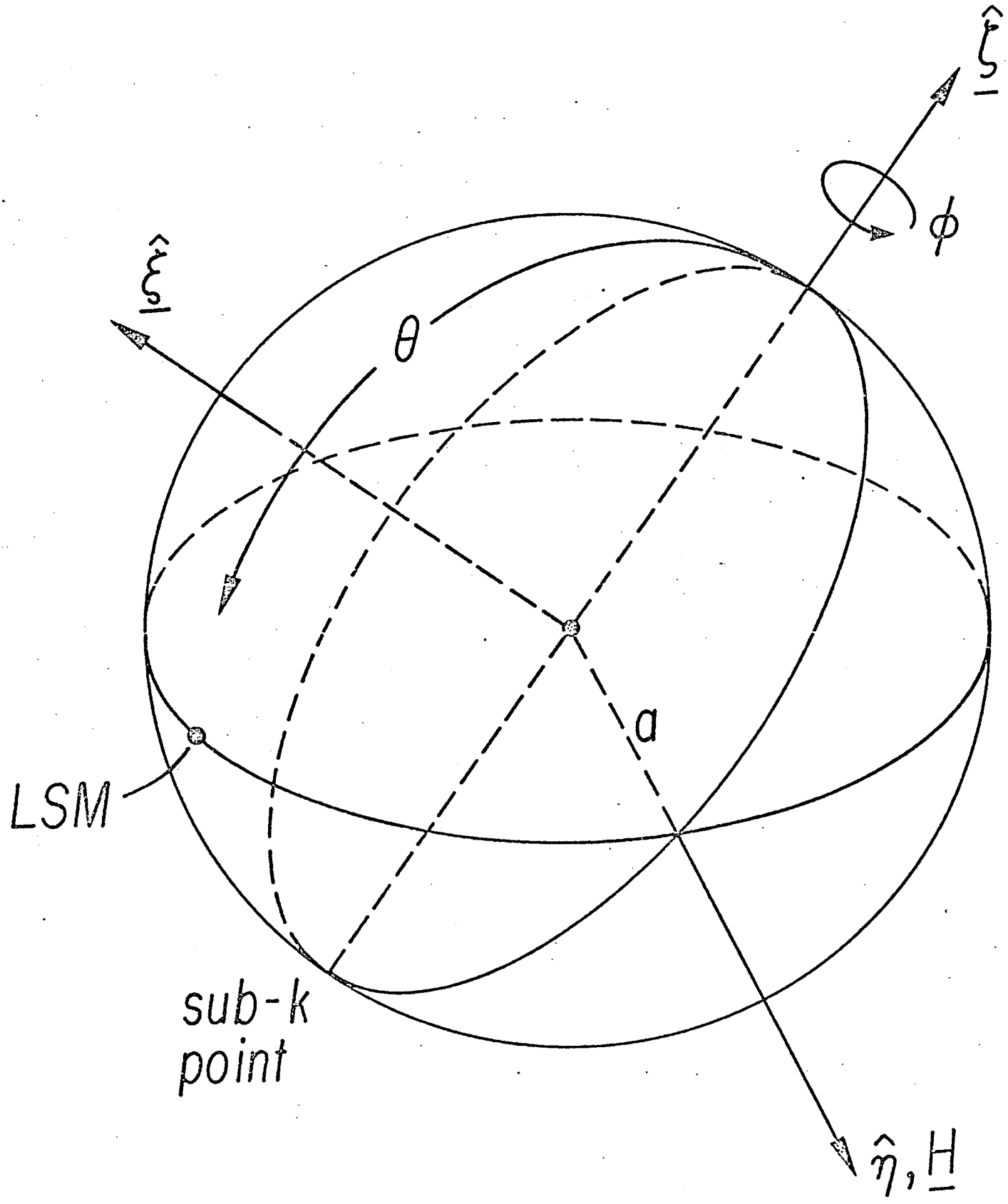

FIG. 2

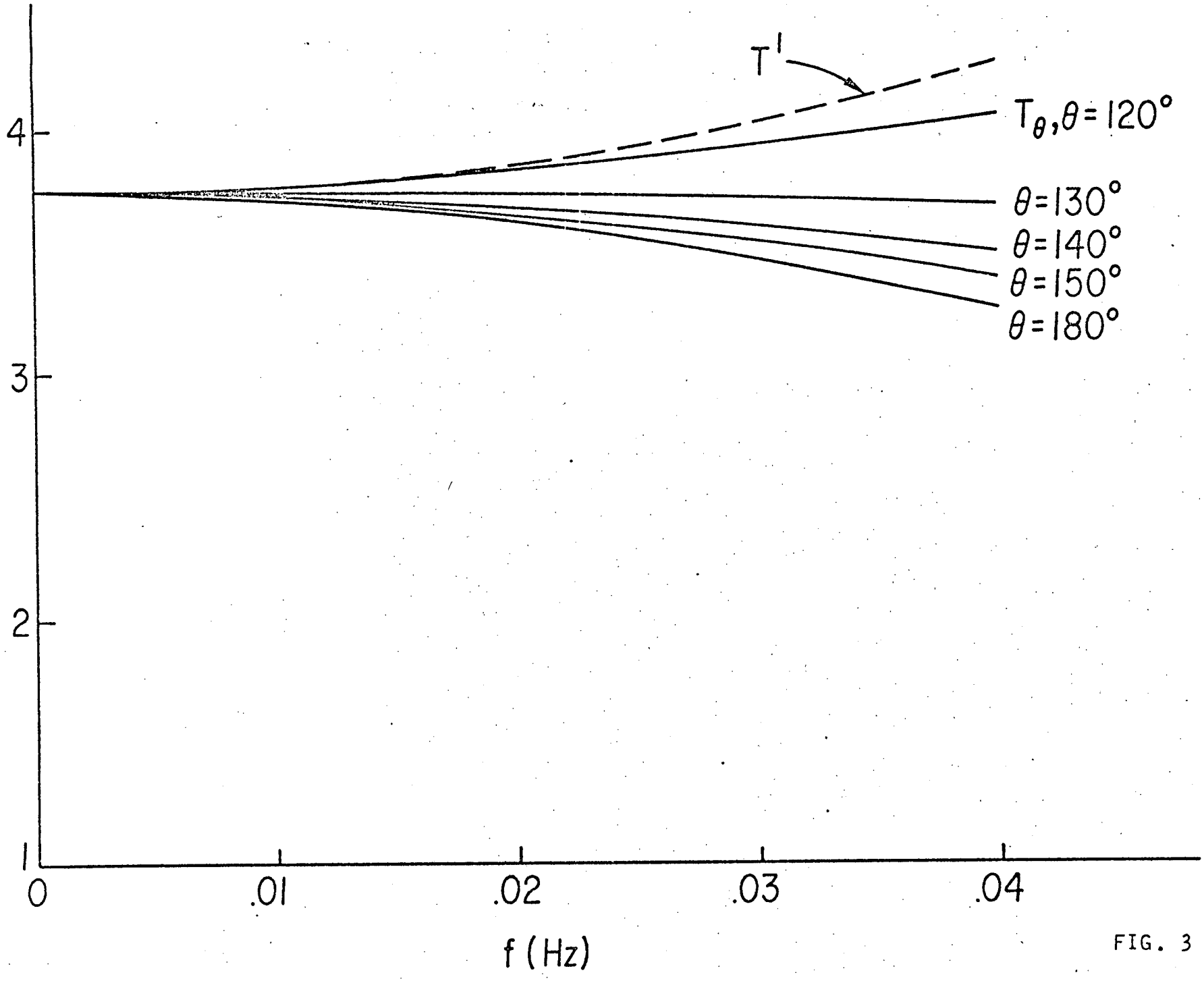
T'
$T_\theta, \theta = 120°$
$\theta = 130°$
$\theta = 140°$
$\theta = 150°$
$\theta = 180°$
4
3
2
1
0
.01
.02
.03
.04
f (Hz)

FIG. 3

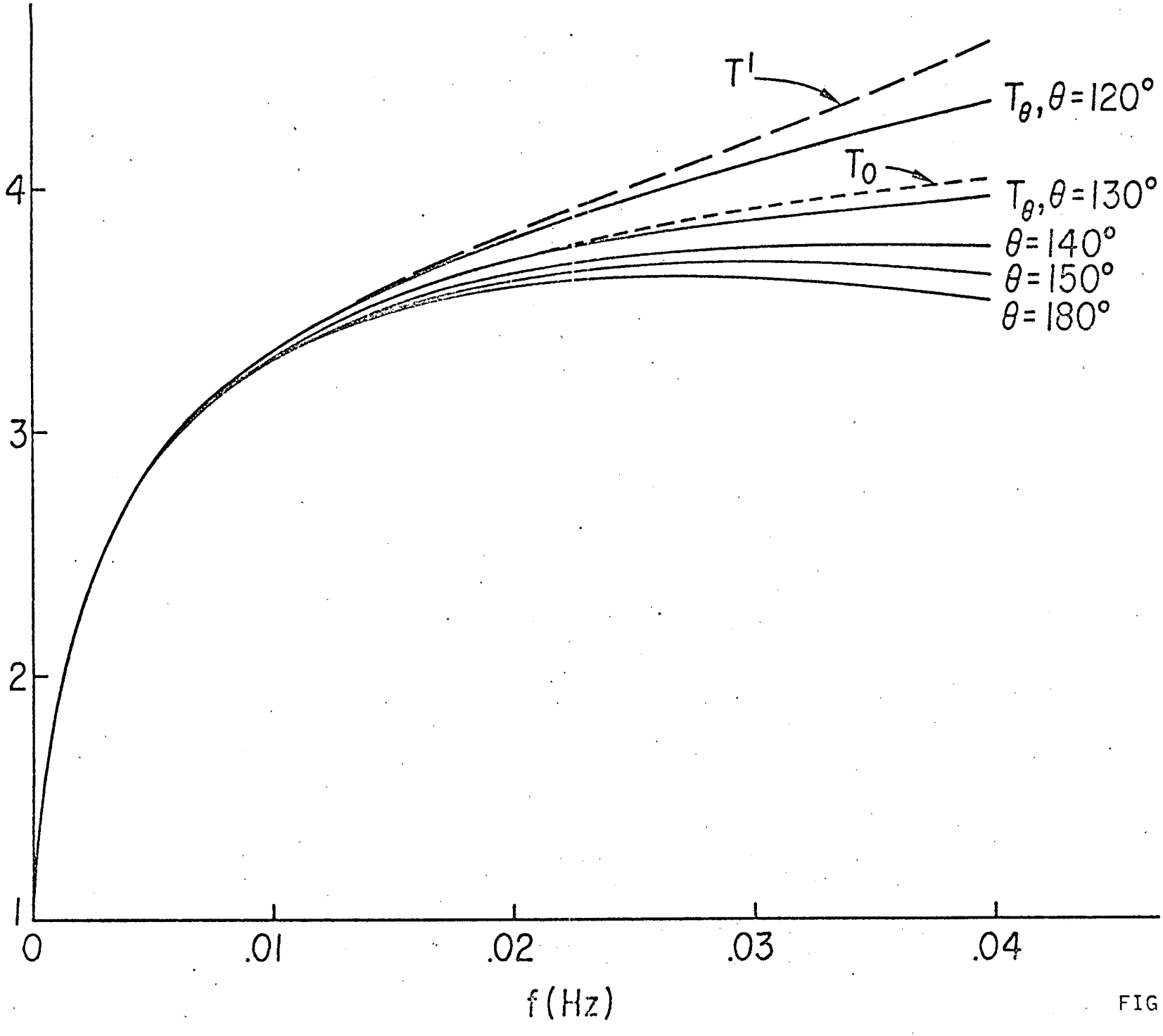
T'
$T_\theta, \theta = 120°$
T_0
$T_\theta, \theta = 130°$
$\theta = 140°$
$\theta = 150°$
$\theta = 180°$
4
3
2
1
0
.01
.02
.03
.04
f (Hz)

FIG. 4

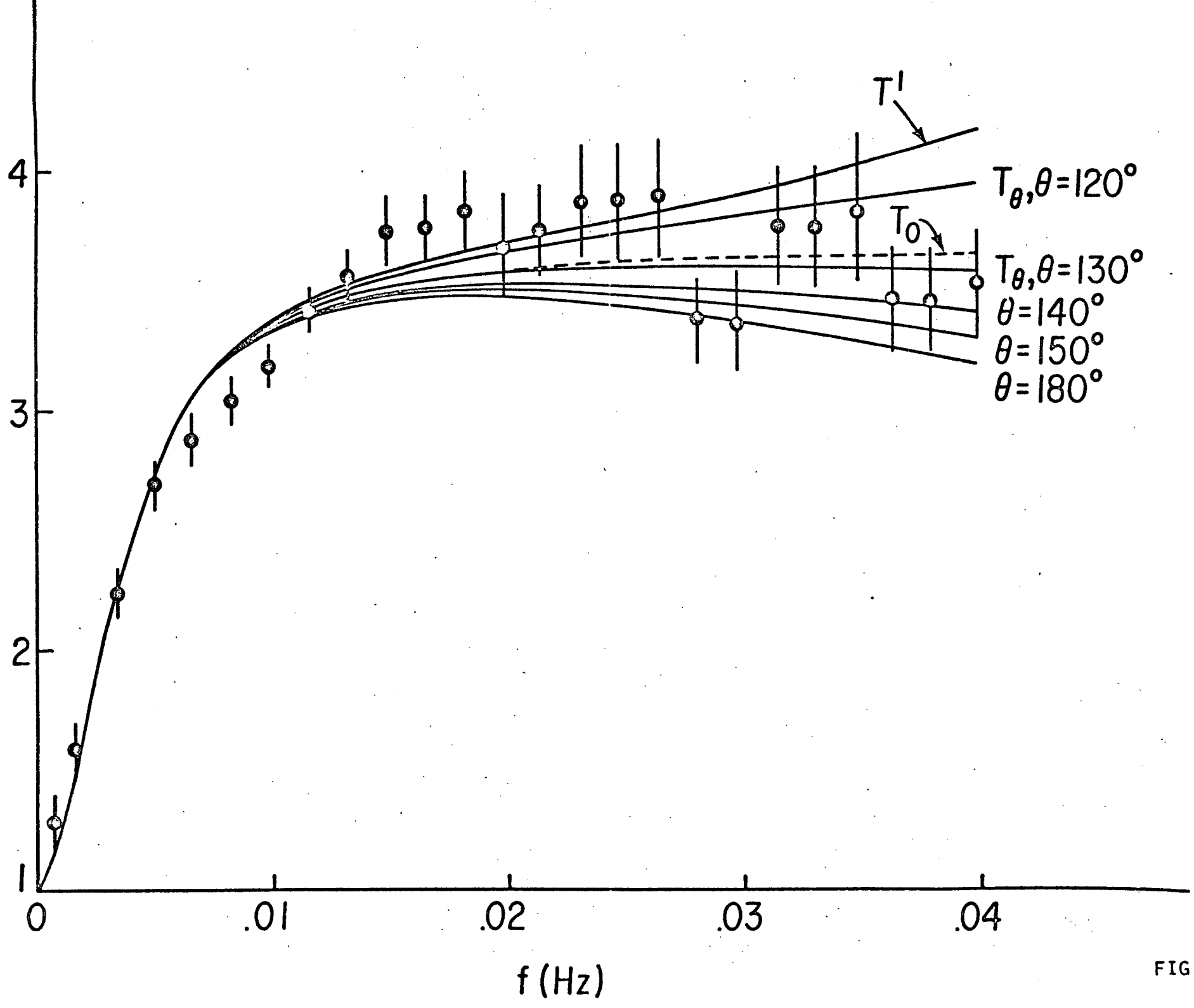
T'
$T_\theta, \theta = 120°$
T_0
$T_\theta, \theta = 130°$
$\theta = 140°$
$\theta = 150°$
$\theta = 180°$
4
3
2
1
0
.01
.02
.03
.04
f (Hz)

FIG. 5